Journal of Alloys and Compounds 780 (2019) 170–176

Contents lists available at ScienceDirect

Journal of Alloys and Compounds

journal homepage: http://www.elsevier.com/locate/jalcom

Synthesis, characterization and electrochemical properties of the layered high capacity sodium ion intercalation cathode material

Yu Wang, Xianyou Wang*, Ruizhi Yu, Xiaohui Zhang, Manfang Chen, Ke Tang, Yan Huang

National Base for International Science & Technology Cooperation, National Local Joint Engineering Laboratory for Key Materials of New Energy Storage Battery, Hunan Province Key Laboratory of Electrochemical Energy Storage & Conversion, School of Chemistry, Xiangtan University, Xiangtan 411105, Hunan, China

ARTICLE INFO

Article history:
Received 9 August 2018
Received in revised form
18 November 2018
Accepted 28 November 2018
Available online 29 November 2018

Keywords:
Sodium ion batteries
Cathode materials
Layered oxides
$NaMn_{2/3}Ni_{1/6}Co_{1/6}O_2$
Phase transitions
Electrochemical performances

ABSTRACT

Because of the high safety, abundant resource and low cost of sodium ion batteries (SIBs), lithium ion batteries (LIBs) will be replaced by SIBs with the ever-increasing market demand for high performance and low cost energy storage battery system. However, the short cycle life and poor rate performance for current SIBs restrict their further application. Cathode materials are the most important component for the development of SIBs, which have an unparalleled effect on enhancing the electrochemical performance of SIBs. Herein, a high electrochemical performance O3-type $NaMn_{2/3}Co_{1/6}Ni_{1/6}O_2$ is synthesized by hydrothermal method and high-temperature annealing. The as-prepared sample shows the uniform spherical morphology and exhibits a specific capacity of 153.6 mAh g^{-1} with high capacity retention of 81.7% after 100 cycles and the coulombic efficiency of 98%. Moreover, the sample also exhibits excellent rate performance and the reversible capacity is 91.6 mAh g^{-1} at 1 C. The remarkably enhancing electrochemical performances make it be considered as a promising cathode active material of SIBs.

1. Introduction

As the global energy crisis worsens, finding clean and sustainable new energy is imperative in contemporary society. At the same time, energy production and storage technologies are increasingly concerned with the rapid development of solar and wind energy technology. Among all various electrical energy storage (EES) technologies, rechargeable batteries are considered as the most commercially viable energy storage technology [1]. As the most suitable power source for portable electronic products, LIBs have received the most widely concerned and research as rechargeable batterie. However, with the large-scale commercial application of LIBs, their disadvantages such as insufficient resources and high costs are gradually exposed. Simultaneously, the advantages of SIBs, such as high safety and sustainability, prompt researchers to use Na^+ to assemble SIB because SIBs have the similar storage mechanism of LIBs [2]. As well as sodium electropositive nature is closer to lithium [3,4], making it become a promising alternative for the development of the next generation of energy storage devices [5]. In addition, Na is more rich in natural abundant (2.64 wt % abundance on Earth) and cheaper than Li [6], therefore SIBs become more prospective energy storage system as a large-scale grid energy storage devices [7].

As we all know, the exploration of SIBs began in the early 1980s [8,9]. During a long period of academic research, the positive electrode is the key factor for restricting the high electrochemical performance of SIBs [10]. The collapse of the structure of the SIBs cathode materials will be occurred during Na^+ intercalation/deintercalation since Na has a larger ionic radius than Li (0.076 vs. 0.102 nm [11]. Therefore, SIBs cathode materials exhibit a poor rate capacity and cycle performance, thus limiting the application of SIBs. Therefore, there is an urgent demand to develop the high electrochemical performance cathode materials of SIBs. During the recent researches on the cathode materials, various functional materials have been proposed and used as cathode materials, including transition-metal oxides, polyanionic compounds, metal hexacyanometalates and organic compounds [12]. Among all materials, transition-metal oxides that are described as Na_xMO_2 (M = Mn, Co, Ni, Fe, etc.) have attracted wide interest as due to the flexibility and versatility of transition-metal oxides [13], and are considered as a kind of promising cathode material for SIBs.

According to the cationic distributions, transition-metal oxides are usually divided into two main categories: layered-Na_xMO_2 and

* Corresponding author.
E-mail address: wxianyou@yahoo.com (X. Wang).

https://doi.org/10.1016/j.jallcom.2018.11.369
0925-8388/

tunnel-$NaMO_2$ [12]. Because of the larger screening effect, sodium has a strong tendency to favor the formation of layered compounds [14]. Therefore, the layered oxides are in dominant proportions in various transition-metal oxides. According to the arrangement of the sodium layer and the transition-metal, layer metal oxides can be classified into two most-common structural polymorphs: P2-phase (Na layers and transition-metal (M) layers stacked in the ABBAABBA manner in which Na^+ and transition-metal ions are individually located in the octahedral sites) and O3-phase (Na layers and transition-metal (M) layers packed closely in the ABCABC pattern, and the Na^+ are all located in the trigonal prismatic sites of the Na layers). When the x values of 0.83–1.0 is the electroactive O3-phase and the x values of 0.67–0.80 is P2-phase [15,16]. Both the P2-Phase and O3-phase can be easily synthesized by co-precipitation reactions, solid-state routes, and hydrothermal methods in air [17–19]. Compared with layered P2 oxides, layered O3 oxides can provide sufficient Na^+ in cells and show higher ion-diffusion coefficients which have been considered as a promising high-energy cathode material of SIB [20]. For instance, as reported, O3-Na_xMnO_2 delivered a capacity of 185 mAh g^{-1} at 0.1 C in the voltage window of 2.0–3.8 V [21]. But P2-$Na_{0.7}MnO_2$ only showed a reversible capacity of 163 mAh g^{-1} and the capacity was 123.95 mAh g^{-1} after 50 cycles (40 mA g^{-1}, 2.0–4.5 V) [17]. The same O3-type compounds such as $NaFeO_2$, Na_xCoO_2 and Na_xNiO_2 showed a high capacity. However, the layer oxides are found to drive several structural phase transitions: O3-O′3-P′3-P3-P′3 during charge and discharge processes [20,22]. Therefore, the materials almost show a significant capacity decay during cyclic process. Besides, because of the layered Na_xMO_2 containing only one transition metal show the poor rate performances. To overcome these issues, combining the various properties of single metal oxides, the research works have been focused on developing multi-metal oxides for SIBs cathode materials. Komaba et al. reported O3-type multi-metal oxides $NaNi_{0.5}Mn_{0.5}O_2$ that showed a stable capacity of 185 mAh g^{-1} when cycled in the voltage window of 2.2–4.5 V. However, the capacity decreased to <100 mAh g^{-1} with 60% capacity retention after 20 cycles [23]. After that, a novel layered oxide material $NaNi_{1/3}Mn_{1/3}Co_{1/3}O_2$ has been reported by Sathiya et al., which delivered 120 mAh g^{-1} at a current density of 0.1 C and exhibited a good capacity retention and rate performance as well after 50 cycles [13]. The good electrochemical performance mainly attributed to manganese, cobalt and nickel in the transition metal (TM) layer. Scrosati et al. reported that $Na[Ni_{0.25}Mn_{0.25}Fe_{0.50}]O_2$ delivered a reversible capacity of 140 mAh g^{-1} at 0.1 C and 85 mAh g^{-1} at 10 C with a capacity retention of 90.4% after 50 cycles in the voltage window of 2.1–3.9 V. The material showed an impressive electrochemical performance [24]. Accordingly, above SIBs cathode materials demonstrate that the multi-metal oxides exhibit better electrochemical performance than that of single metal oxides.

Herein, based on various electrochemical advantages of single metal oxides, such as the excellent stability of Na_xMnO_2, the high specific capacity of Na_xNiO_2 and good ionic diffusion of Na_xCoO_2 [12]. And combined the advantages of O3-phase oxides and multi-metal oxides, a high electrochemical performance spherical O3 oxide (Na/M > 0.67) cathode material $NaMn_{2/3}Ni_{1/6}Co_{1/6}O_2$ (space group: *R3m*, denoted hereafter NaMCN) was prepared by hydrothermal method and subsequently annealing process. The as-prepared sample delivers a high initial discharge capacity of 152 mAh g^{-1} at 0.1 C in the potential range of 2.0–4.2 V and a good cycling performance as well as capacity retention of 81.7% after 100 cycles. The coulombic efficiency is about 97%.

2. Experiment section

Layered NaNMC was synthesized by a high temperature reaction from sodium carbonate and a manganese-cobalt-nickel oxide precursor. The precursor is obtained by hydrothermal and sintering. Three metal chlorates salts (Mn, Ni, and Co; Aldrich 99%) in a mole ratio of 4:1:1 which were dissolved into ethylene glycol under stirring. After getting a transparent solution, the excess ammonium bicarbonate was added into the solution under stirring for two hours. Then mixture was transferred to the hydrothermal reactor and reacted at 180 °C for 15 h in a high temperature oven. After the reaction is completed, the solution is filtered to give a light red precipitate $Mn_2Co_{0.5}Ni_{0.5}CO_3$, then the precipitate was washed three times with deionized water and ethanol and dried at 60 °C for 12 h in an oven. The dried material was calcined at 500 °C for 6 h in an open-air muffle furnace with 2 °C/min to synthetic precursor: $Mn_2Co_{0.5}Ni_{0.5}O_2$. The precursor and Na_2CO_3 (sodium: transition-metal = 1.05:1) mixed by grinding with alcohol for 30 min, then the mixture was dried at 60 °C for 1 h and calcined at 700 °C for 10 h in a muffle furnace with 3 °C/min. The product finally stored under inert atmosphere(see Fig. 1).

2.1. Characterization

The accurate chemical composition of the product was analyzed by an inductively coupled plasma optical emission spectrometer (ICP-OES, Agilent-725, Australia). The crystalline structure was characterized by X-ray diffraction (XRD, Model D8-Advance Germany) using the Cu Kα radiation (λ = 1.5418 Å) at 40 kV and 40 mA over the 2θ range from 10° to 90°. The lattice parameters were determined using the refinement software, General Structure Analysis System (GSAS) code. The particle morphology and particle

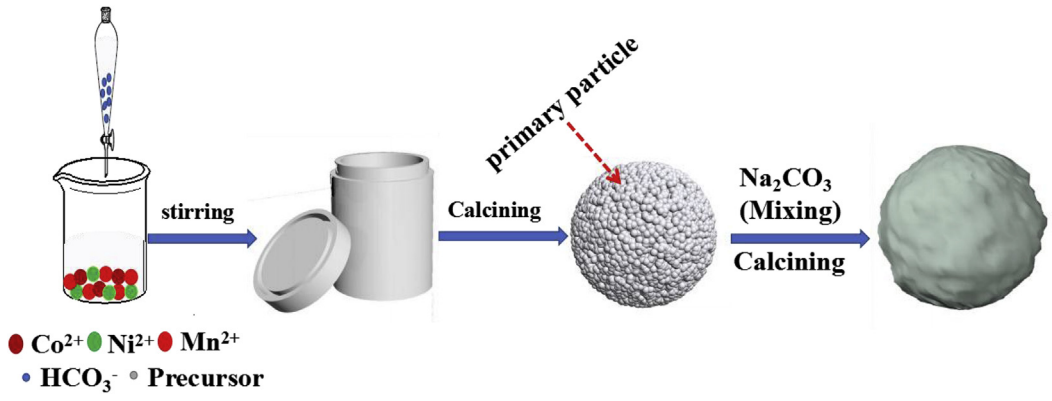

Fig. 1. Schematic illustration for the designed route to synthesize NaMCN microspheres.

size distribution studies were carried out with field emission scanning electron microscope (FESEM, Hitachi S-4800). The microstructure and element distribution of particle was observed by high resolution transmission electron microscopy and the EDX mapping (JEM-2100F microscope operating at 200 kV). The element valence was determined by X-ray photoelectron spectroscopy (XPS, K-Alpha1063, Japan).

2.2. Electrochemical measurement

Positive electrodes were prepared by mixing 10 wt % of Acetylene black, 80 wt % of active material and 10 wt % of PVDF in N-methyl-2-pyrrolidone (NMP) and coating the slurry on Al foil. The active material mass loading in the electrodes was about 2 mg cm^{-2}. The button cells were assembled in an argon filled glovebox. Sodium metal was used as counter and reference electrodes, and the metal sodium was cut from sodium chunks (99.8%, Aladdin) and then made into sodium tablets. The positive electrodes separated from the negative electrode 3 sheets of glass fiber disks which are soaked with a 1 M solution of $NaClO_4$ in an ethylene carbonate (EC)/Propylene carbonate (PC) mixture (1/1 v/v). Cells were cycled galvanostatically at different constant current rates (theoretical capacity = 240 mAh g^{-1}, 1 C = 240 mA g^{-1}) between 2.0 and 4.2 V in Neware battery tester (BTS-XWJ-6.44S-00052 Neware, Shenzhen, China). Cyclic voltammetry (CV) tests were performed at a scan rate of 0.1 mV s^{-1} between 2.0 and 4.2 V (vs Na^+/Na). CV were conducted using an electrochemical workstation (CHI660e Chenhua, China) The EIS was also recorded using the CHI over the frequency range from 10 mHz to 100 kHz, while the disturbance amplitude was 5 mV. All the electrochemical measurements were carried out at 25 °C.

3. Results and discussion

The elemental composition of the material was deduced from ICP-OES analysis result. The relative elements ratio of Na, Mn, Co and Ni was Na: Mn: Co: Ni = 1.03: 0.674: 0.173: 0.157 for NaMCN. The sodium and transition metal ratio of the material is in a good consistent with designed sample. Hence, the material can be described as $NaMn_{2/3}Co_{1/6}Ni_{1/6}O_2$.

The results of powder X-ray diffraction (XRD) of NaNMC are shown in Fig. 2. The Rietveld refinement is calculated on the Na_xCoO_2 model structure with rhombohedral symmetry (*R*-3*m* space group PDF No: 01-070-2030). As shown in Fig. 2 the observed pattern is consistent with the calculated pattern. The impurity peaks corresponding to sodium salts and manganese, cobalt or nickel oxides are not observed. The parameters R_p, R_{wp}, and χ^2, where R_p and R_{wp} are the profile and weighted profile R-factors, and χ^2 is the goodness-of-fit parameter, are 4.13%, 5.37%, and 4.65%, respectively. The calculated lattice parameters are a = b = 2.8528 (5) Å and c = 16.7676 (4) Å, respectively. The ellipse region identified in the picture shows a very weak peak which cannot match the calculated theoretical peak position. By comparison, the weak peak may originate from the P3 phase (*R*-3*m* space group). The formation of P3 phase is due to a long time high temperature sintering, but the proportion of P3 phase is too small to affect the electrochemical performance of the NaMCN. In general, the detected crystal information is well matched with the ideal O3-type layered structure model. The XRD pattern confirms the materials with the space group *R*-3*m*.

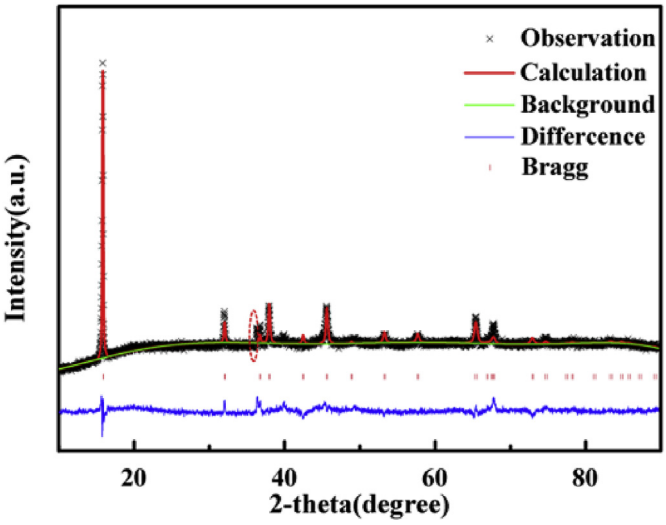

Fig. 2. X-ray diffraction pattern and Rietveld refinement of NaMCN.

The morphologies of the as-prepared precursor and NaMCN are shown in Fig. 3(a) and (b). As shown in Fig. 3(a), the size of precursor powder is average about 1 μm with regular spherical morphology. Each spherical particle is made up of primary nanoparticles of similar size. The primary nanoparticles are the same as the flake shape of brucite and the particles size is about 200 nm. As shown in Fig. 3(b), the NaMCN sample also shows a uniform spherical morphology. However, the particles show a slightly agglomeration and the particle size slightly grows up. In addition, the pore structure on the surface of the NaMCN sample is disappeared and the surface and edges of NaMCN become smooth, which will improve the tap density of the material. The structure of NaMCN is further characterized by transmission electron microscope (TEM) in Fig. 3(c). The results obtained from TEM correlate well with SEM results. Fig. 3(d) and (e) show the fast Fourier transform (FFT) pattern and representative high-resolution TEM image. Fig. 3(e) shows the crystal lattice fringe spacing is 2.47 Å, which is assigned to the (101) lattice plane and planes lattice spacing of (012) indexed as 2.38 Å of NaMCN. The (101) planes of the *R*-3*m* layered structure prove that the material is a layered structure, and it is consistent with the XRD refinement results. The distribution of elements in the NaMCN was characterized by EDX-mapping. Fig. 3(f–j) show EDX-mapping results, the sodium, manganese, cobalt, nickel and oxygen demonstrate a similar homogeneous distribution in the all measured area.

XPS measurements show the more information about the oxidation state of transition metal ions in the layered NaMCN. The corresponding spectra are shown Fig. 4. Through referencing the C 1s line to 284.85 eV to correct the binding energies for specimen charging. The presence of Na, Mn, Co, Ni and O as well as C from the reference and the absence of other impurity are proved by the survey spectra as shown in Fig. 4(a). The dominant peaks in which binding energies are 780.0, 563.8 and 855.7 eV are attributed to Co^{3+}, Mn^{4+} and Ni^{2+}, respectively [25]. Fig. 4(b) shows the Ni 2p XPS spectrum, the peak located at about 854.3 eV is assigned to Ni $2p_{3/2}$ and a small peak at about 862.0 eV is corresponded to Ni (II) cation. There is a less prominent peak at 855 eV, it indicates the existence of Ni^{3+} [26]. Fig. 4(c) shows the Co 2p spectrum, there are two major peaks at 780 and 795 eV which assigned to the Co $2p_{3/2}$ and Co $2p_{1/2}$, respectively. The pattern shows a fingerprint of Co (III) cation, which is the two weak shake-up satellite peaks correspond to a binding energy values of 789.7 and 805.6 eV, respectively. These results confirm the existence of the Co (III) [27], The two weak peaks emerge at 782.0 and 797.1 eV indicate the existence of Co (II) after refined fitting. The two main spin-orbit lines of 2p1/2 at 654.3 eV and $2p_{3/2}$ at 643.0 eV with separation of 11.3 eV in Fig. 4(d), which illustrate the dominant Mn (IV) cation. However,

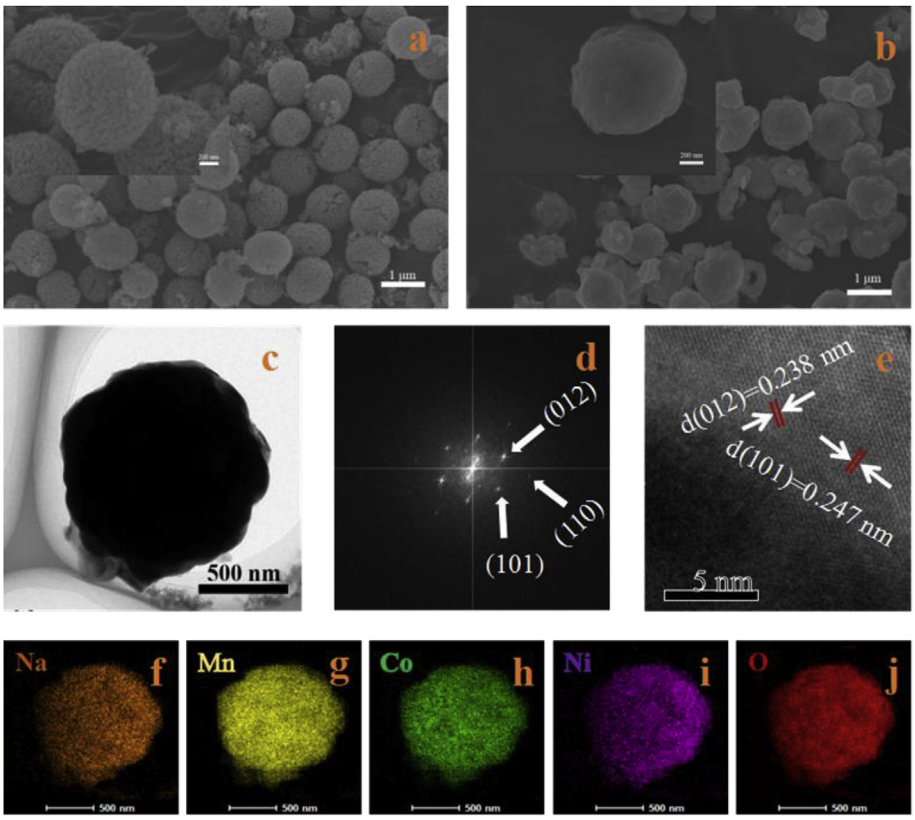

Fig. 3. (a) SEM image of $Mn_2Co_{0.5}Ni_{0.5}O_2$, (b) SEM image of NaMCN cathode material, (c) TEM image of NaMCN, (d) HRTEM image of NaMCN and (e) the fast Fourier transform pattern, (f–j) distribution of elements in the NaMCN.

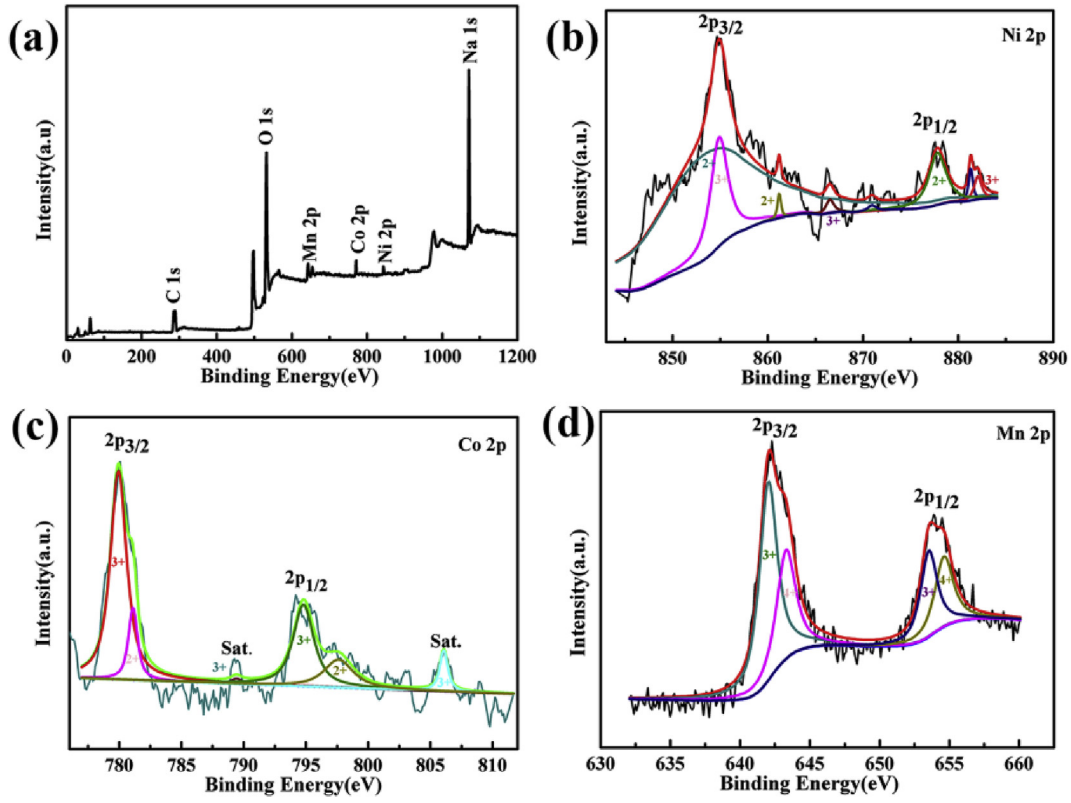

Fig. 4. XPS spectra of (a) survey spectrum, (b) Ni 2p, (c) Co 2p and (d) Mn 2p for NaMCN.

there are a couple of less obvious peaks at 644 and 653.8 eV are observed and these are corresponds to Mn (III) cation [28].

The existence of Mn^{3+} and Ni^{3+} in transition-metal ions is attributed to the electron transfer between Ni^{2+} and Mn^{4+} ion pairs leading to valency-degeneracy by the dynamic equilibrium reported by Shaju et al. [29]. The XPS result proves that the majority oxidation states are in 2 + and 4 + of Ni and Mn ions in NaMCN. Moreover, Ni^{3+} and Mn^{3+} ions in the lattice may be caused by valence degradation. The Ni^{2+} and Co^{3+} cations could be assigned to the electrochemically active transition metal ions which undergo redox transitions during Na^+ intercalation/deintercalation. While Mn^{4+} cations are assigned to electrochemically inactive and they are considered to enhance the stability of the sample material structure [30,31]. Thus, the above result indicates that NaMCN has a stable structure and good electrochemical activity.

The electrochemical performance of NaNMC is tested by assembling sodium half cells. The electrochemical properties of NaMCN sample is first investigated by CV. Fig. 5(a) shows the CV curves of the NaMCN electrode between 2.0 and 4.2 V versus Na^+/Na at the scan rate of 0.1 mV s^{-1}. The half cells show an open circuit potential of 2.8 V. It is normal NaMCN vs Na cells in the voltage range of 2.0–4.2 V. From CV curves, it can be found that there is a pair of prominent oxidation/reduction peaks at 3.5/2.3 V and a wide reduction peak at 3.2 V corresponding to the Ni^{2+}/Ni^{3+} and Ni^{3+}/Ni^{4+} redox couples [32]. It is known that the multiphase transformation is harmful to maintain the cathode structure stability during Na^+ intercalation/deintercalation, especially the phase transitions of O3-P3 and P3-O1 are the main factors leading to the poor cycling performance of O3-type materials [33]. The reduction/oxidation peaks at 3.10/3.42 V and 3.58/3.70 V (Na^+/Na), corresponding to the O3-P3 and P3-O1 phase transitions, which are not observed in CV curves. It indicates that O3-P3 and P3-O1 phase transformation is availably restrained. Besides, no other peaks are found, implying a series of other phase transitions with intermediate phase do not occur during Na^+ insertion/extraction processes, thus suggesting that the multiphase transformation is intentionally inhibited [34]. The close overlapping of the CV curves confirm a high reversibility of sodiation/de-sodiation. Thus, the cycling and

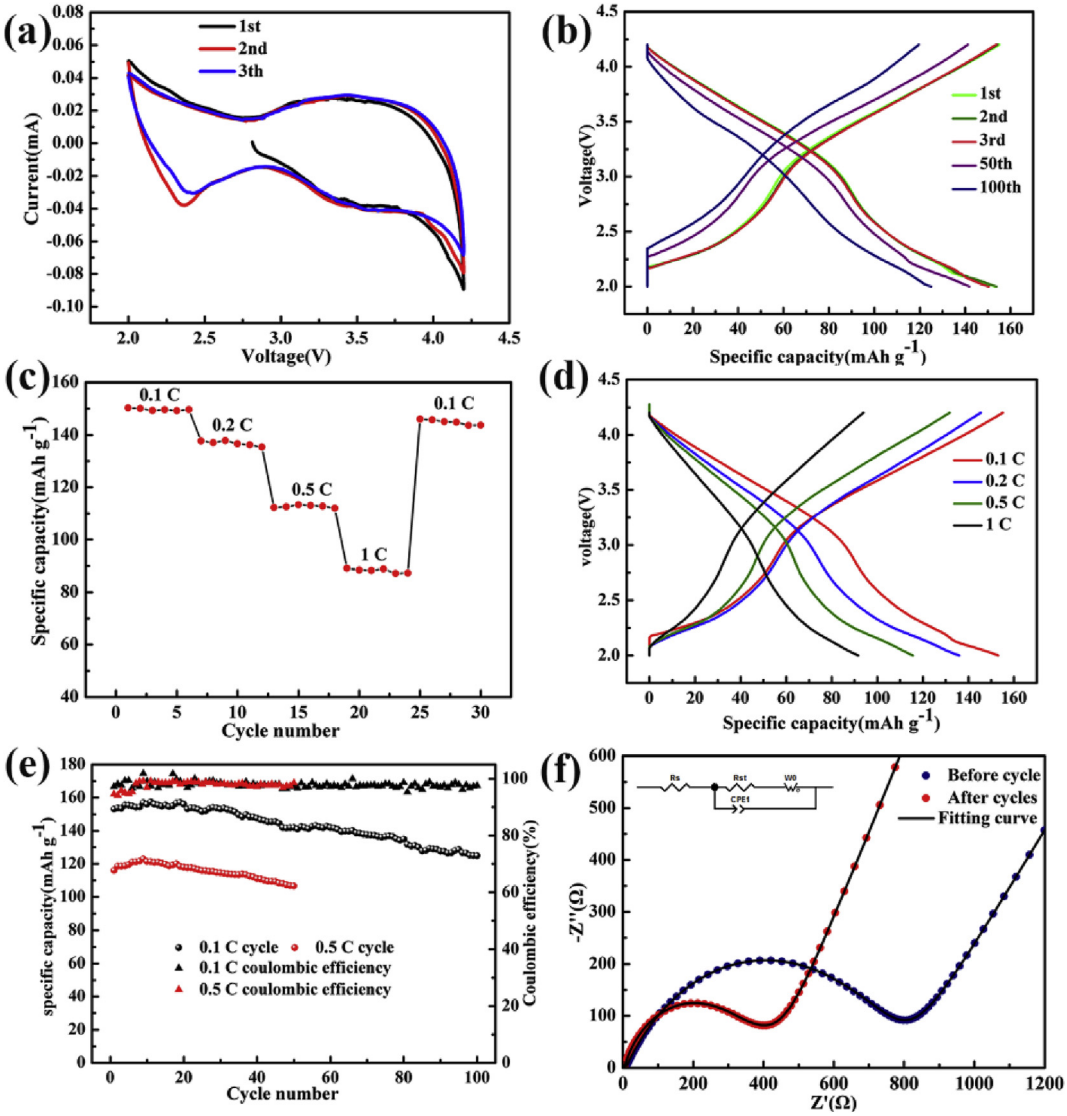

Fig. 5. (a) Cyclic voltammograms for the first three cycles at a scan rate of 0.1 mV s^{-1}, (b) charge and discharge curves of NaMCN electrode between 2.0 and 4.2 V versus Na^+/Na at selected cycles at 0.1 C, (c) rate performance from 0.1 to 0.5 C, (d) charge and discharge curves for the first cycle at 0.1, 0.2, 0.5, and 1 C, (e) cycling performance at 0.1 and 0.5 C, (f) Nyquist plots of NaMCN recorded at open circuit voltage.

rate performances of NaMCN could be efficiently improved.

Fig. 5(b) shows the charge and discharge performance of NaMCN as a cathode material. As shown in Fig. 5(b), when cycled at 0.1 C, the NaMCN sample exhibits the initial charge and discharge capacities of 157.1 and 153.6 mAh g^{-1}, respectively as well as the coulombic efficiency of 97.3%. The initial discharge specific capacity is higher than that of $NaMn_{1/3}Co_{1/3}Ni_{1/3}O_2$, which has been reported by Sathiya et al. [13]. Furthermore, it can be seen from corresponding CV curves that there is no obvious charge and discharge platform at 2.3 V and 3.5 V, so this further demonstrates that there is no O3-P3 phase transformation. The solution reaction during Na extraction and insertion creates the sloping region [35]. The discharge capacity for the 2nd, 3rd, 50th and 100th are 153.2, 151.7, 141.2 and 124.9 mAh g^{-1}, respectively. According the charge profile, the capacity fading only derives from high voltage (>3.25 V), which is may be assigned to the catalytic decomposition of Na-based electrolyte and the structure irreversibility of the NaMCN at high voltage.

Fig. 5(c) illustrates a C-rate test, the current densities from 0.1 C to 1 C within 2.0–4.2 V. When coming back the current density of 0.1 C again, the discharge capacity could be almost recovered to 150 mAh g^{-1}, which proves that NaMCN possesses a good rate performance and excellent cyclic stability. The structure of NaMCN is stable because special spherical shape can withstand the changes of high stress during Na intercalation/deintercalation processes at high current densities. Compared with the same type of materials [12]. NaMCN sample shows an improved rate performance, indicating an improved kinetics. Such excellent cycling and rate performance suggest that O3-NaMCN will be a promising cathode material for SIBs. The selected charge/discharge curves at the 0.1, 0.2, 0.5 and 1 C rates of NaMCN are presented in Fig. 5(d). The reversible capacities are 153.6, 135.9, 115.6 and 91.6 mAh g^{-1}, respectively. In addition, when the current density increases, even though more obvious electrode polarization of NaMCN sample is observed, the polarization is the smallest compared with the same type of electrode materials [36]. The coulombic efficiencies are close to 100% during cycling at 0.2, 0.5 and 1 C, which indicates that the insertion process is not limited. However, the electrode polarization presents a slight growth at different rates, which indicates that the resistance of Na^+ diffusion increases at high current density.

The cycling performances of NaMCN at 0.1 C and 0.5 C are shown in Fig. 5(e). When the NaMCN sample cycles at 0.1 C, the electrode delivers a capacity of about 125 mAh g^{-1} after 100 cycles, corresponding to capacity retention of 81.7%. Despite NaMCN sample displays a certain capacity fading, the cyclic stability of NaMCN still exceeds the same type of material [12]. When the NaMCN sample cycles at 0.5 C after 50 cycles, the capacity is still 106.7 mAh g^{-1}, which exhibits remarkable cyclic stability. The coulombic efficiency exceeds 97% during cycling except in the initial 10 cycles, and it shows that there is an activation process at high current densities. It is possible that side reactions occurred between the electrolyte and the electrode surface during the first ten cycles and SEI film formed [34]. At a current density of 0.5 C after activation, the material discharge capacity quickly stabilized at 122 mAh g^{-1}, which indicates the NaMCN sample could facilitate the formation of a uniform SEI faster and suppress side reactions between the electrolyte and the cathode. The enhanced cyclic stability of NaMCN is associated with a part of electrochemically active 3d TM ions Co^{3+} and Ni^{3+} in the TM layers, and cobalt existence is beneficial to in improving NaMCN electrochemical performance owing to the synergistic effect for various metal ions [12,36]. Furthermore, the good electrochemical behavior may stem from its even distribution and uniform particle size, resulting in shorting Na^+ diffusion length and enabling better contact between electrolyte and active particles. Thus, special spherical structure enhanced the electrochemical performance of Na^+ storage. Moreover, the Mn^{4+} oxidation state and the presence of strong Mn/Ni-O bonds can improve the structural stability [37]. The performance comparisons of $NaMn_{2/3}Co_{1/6}Ni_{1/6}O_2$ with other similar materials are shown in Table 1. The results demonstrate that NaMCN has higher capacity and better cycle stability than the same type of materials.

In addition, the electrochemical impedance spectroscopy (EIS) measurements are finished and fitted using the equivalent circuit given in Fig. 5(f). EIS measurements are carried out before cycle and after 100 cycles at 0.1 C. A slope line at low frequency and a semicircle at high frequency form the EIS plots. Generally speaking, the charge transfer resistance (R_{ct}) is the semicircle at the higher frequency range, which is associated with the electrochemical kinetics of material. The Warburg impedance (Z_w) is reflected by the slop line at low frequency range, which is related to Na + diffusion in the particles of the electrode material. In addition, the uncompensated ohmic resistance (R_s) is the intercept of the semicircle in the high frequency region with the Z′ real axis. It corresponded to the resistance between the electrolyte and cathode interface. As seen from Fig. 5(f), the NaMCN cell exhibits an a R_s value of about 8 Ω before cycle. After 100 cycles, the NaMCN exhibits a R_s value of 3 Ω. The value of R_s is smaller than that of similar cathode materials [12] indicating that NaMCN could form the stable solid-electrolyte interfacial layer during charge-discharge process. The EIS shows R_{ct} value of about 735 Ω before cycle and R_{ct} value of 345 Ω after 100 cycles. NaMCN shows a lower R_{ct}, which corresponds to the high conductivity and good correlation with the rate performance studies. A lower impedance value and the high conductivity demonstrate that NaMCN sample will render to an excellent electrochemical performance.

4. Conclusions

A high electrochemical performance O3-type $NaMn_{2/3}Ni_{1/6}Co_{1/6}O_2$ cathode material for the application of sodium ion battery was successfully synthesized via hydrothermal method and annealing

Table 1
The performance comparisons of $NaMn_{2/3}Co_{1/6}Ni_{1/6}O_2$ with some other similar materials.

Material	Phase	Practical capacity [mAh g^{-1}]	Capacity retention	Reference
$NaMn_{1/3}Ni_{1/3}Co_{1/3}O_2$	O3	120 (0.1 C, 2.0–3.75 V)	96% (50 cycles)	[13]
$NaNi_{0.5}Co_{0.2}Mn_{0.3}O_2$	O3	164.8 (0.05 C, 2.0–4.25 V)	97.5% (50 cycles)	[38]
$Na_xNi_{0.22}Co_{0.11}Mn_{0.66}O_2$	P2	147.2 (0.1 C, 2.1–4.3 V)	58.8% (200 cycles)	[39]
$Na_{2/3}Co_{2/3}Mn_{2/9}Ni_{1/9}O_2$	P2	110 (0.05 C, 2.0–4.2 V)	89% (90 cycles)	[40]
$Na_{0.67}Ni_{0.4}Co_{0.2}Mn_{0.4}O_2$	P2	124 (0.1 C, 1.5–4.2 V)	61% (55 cycles)	[41]
$Na_{0.67}Mn_{0.65}Ni_{0.15}Co_{0.2}O_2$	P2	141 (0.1C, 2.0–4.3 V)	88.6% (50 cycles)	[42]
$Na_{2/3}Mn_{0.54}Ni_{0.13}Co_{0.13}O_2$	P2	120 (0.1 C, 2.0–4.5 V)	50% (100 cycles)	[43]
$Na_{2/3}Mn_{0.55}Ni_{0.30}Co_{0.15}O_2$	P2	120 (0.1 C, 2.0–4.0 V)	82% (50 cycles)	[44]
$NaMn_{2/3}Co_{1/6}Ni_{1/6}O_2$	O3	153.6 (0.1 C, 2.0–4.2 V)	81.7% (100 cycles)	

process. The $NaNaMn_{2/3}Co_{1/6}Ni_{1/6}O_2$ exhibited an initial specific discharge capacity of 153 mAh g^{-1} at 0.1 C with capacity retention of 81.7% after 100 cycles. A remarkable rate performance is obtained after 50 cycles at 0.5 C with good capacity retention of 92.3%. It can be considered that a part of Co^{3+} and Ni^{3+} in the TM layers could improve structure stability during Na^+ intercalation/deintercalation processes. Moreover, the introduction of Co^{3+} can reduce the mixed cation occupying, increase the diffusion rate of Na^+, enhance the conductivity, and improve cycle and rate performance of sample. In the same time, NaMCN could suppress the occurrence of multi-phase transitions, and there is a wide voltage window (2.0–4.2 V). As a result, $NaMn_{2/3}Co_{1/6}Ni_{1/6}O_2$ will be a promising high-performance cathode material for the application of SIBs.

Acknowledgement

This work is supported financially by the National Natural Science Foundation of China under project (No. 51272221), the Key Project of Strategic New Industry of Hunan Province under project (No. 2016GK4005 and 2016GK4030).

References

[1] M.S. Dresselhaus, I.L. Thoms, Alternative energy technologies, Nature 414 (2001) 332.
[2] M.D. Slater, D. Kim, E. Lee, C.S. Johnson, Sodium-ion batteries, Adv. Funct. Mater. 23 (2013) 947–958.
[3] S.W. Kim, D.H. Seo, X. Ma, G. Ceder, K. Kang, Electrode materials for rechargeable sodium-ion batteries: potential alternatives to current lithium-ion batteries, Adv. Energy Mater. 2 (2012) 710–721.
[4] B.L. Ellis, L.F. Nazar, Sodium and sodium-ion energy storage batteries, Curr. Opin. Solid State Mater. Sci. 16 (2012) 168–177.
[5] M.M. Doeff, S.J. Visco, Y.P. Ma, M. Peng, L. Ding, J.H. De, Thin film solid state sodium batteries for electric vehicles, Electrochim. Acta 40 (1995) 2205–2210.
[6] D. Buchholz, A. Moretti, R. Kloepsch, S. Nowak, V. Siozios, M. Winter, S. Passerini, Toward Na-ion batteries-synthesis and characterization of a novel high capacity Na ion intercalation material, Chem. Mater. 25 (2013) 142–148.
[7] G. Wang, X. Xiong, D. Xie, Z. Lin, J. Zheng, F. Zheng, Y. Li, Y. Liu, C. Yang, M. Liu, Chemical activated hollow carbon nanospheres as a high-performance anode material for potassium ion batteries, J. Mater. Chem. A (2018), https://doi.org/10.1039/C8TA09751H.
[8] S. Miyazaki, S. Kikkawa, M. Koizumi, Chemical and electrochemical deintercalations of the layered compounds $LiMO_2$ (M= Cr, Co) and $NaM'O_2$ (M' Cr, Fe, Co, Ni), Synth. Met. 6 (1983) 211–217.
[9] S. Miyazaki, S. Kikkawa, M. Koizumi, Electrochemical aspects of the deintercalation of layered AMO_2 compounds, J. Power Sources 14 (1985) 231–234.
[10] Y. You, A. Manthiram, Progress in high-voltage cathode materials for rechargeable sodium-ion batteries, Adv. Energy Mater. 8 (2018), 1701785.
[11] Y. Fang, L. Xiao, Z. Chen, X. Ai, Y. Cao, H. Yang, Recent advances in sodium-ion battery materials, Electrochem. Energy Rev. (2018) 1–30.
[12] X. Xiang, K. Zhang, J. Chen, Recent advances and prospects of cathode materials for sodium-ion batteries, Adv. Mater. 27 (2015) 5343–5364.
[13] M. Sathiya, K. Hemalatha, K. Ramesha, J.M. Tarascon, A.S. Prakash, Synthesis, structure, and electrochemical properties of the layered sodium insertion cathode material: $NaNi_{1/3}Mn_{1/3}Co_{1/3}O_2$, Chem. Mater. 24 (2012) 1846–1853.
[14] M.H. Han, E. Gonzalo, G. Singh, T. Rojo, A comprehensive review of sodium layered oxides: powerful cathodes for Na-ion batteries, Energy Environ. Sci. 8 (2015) 81–102.
[15] C. Delmas, J.J. Braconnier, C. Fouassier, P. Hagenmuller, Electrochemical intercalation of sodium in Na_xCoO_2 bronzes, Solid State Ionics 3 (1981) 165–169.
[16] R.J. Clément, P.G. Bruce, C.P. Grey, Review-manganese-based P2-type transition metal oxides as sodium-ion battery cathode materials, J. Electrochem. Soc. 162 (2015) A2589–A2604.
[17] J. Billaud, R.J. Clement, A.R. Armstrong, J. Canales-Vazquez, P. Rozier, C.P. Grey, P.G. Bruce, beta-$NaMnO_2$: a high-performance cathode for sodium-ion batteries, J. Am. Chem. Soc. 136 (2014) 17243–17248.
[18] A. Caballero, L. Hernán, J. Morales, L. Sánchez, J. Santos Peña, M.A.G. Aranda, Synthesis and characterization of high-temperature hexagonal P2-$Na_{0.6}MnO_2$ and its electrochemical behaviour as cathode in sodium cells, J. Mater. Chem. 12 (2002) 1142–1147.
[19] D. Su, C. Wang, H.J. Ahn, G. Wang, Single crystalline $Na_{0.7}MnO_2$ nanoplates as cathode materials for sodium-ion batteries with enhanced performance, Chem. Eur. J. 19 (2013) 10884–10889.
[20] C. Delmas, Sodium and sodium-ion batteries: 50 Years of research, Adv. Energy Mater. 8 (2018), 1703137.
[21] X. Ma, H. Chen, G. Ceder, Electrochemical properties of monoclinic NaMnO2, J. Electrochem. Soc. 158 (2011) A1307.
[22] Y. Lei, X. Li, L. Liu, G. Ceder, Synthesis and stoichiometry of different layered sodium cobalt oxides, Chem. Mater. 26 (2014) 5288–5296.
[23] S. Komaba, N. Yabuuchi, T. Nakayama, A. Ogata, T. Ishikawa, I. Nakai, Study on the reversible electrode reaction of $Na_{1-x}Ni_{0.5}Mn_{0.5}O_2$ for a rechargeable sodium-ion battery, Inorg. Chem. 51 (2012) 6211–6220.
[24] S.M. Oh, S.T. Myung, C.S. Yoon, J. Lu, J. Hassoun, B. Scrosati, K. Amine, Y.K. Sun, Advanced $Na[Ni_{0.25}Fe_{0.5}Mn_{0.25}]O_2$/C-$Fe_3O_4$ sodium-ion batteries using EMS electrolyte for energy storage, Nano Lett. 14 (2014) 1620–1626.
[25] N.N. Sinha, N. Munichandraiah, Synthesis and characterization of carbon-coated $LiNi_{1/3}Co_{1/3}Mn_{1/3}O_2$ in a single step by an inverse microemulsion route, ACS Appl. Mater. Interfaces 1 (2009) 1241–1249.
[26] A.N. Mansour, Characterization of $LiNiO_2$ by XPS, Surf. Sci. Spectra 3 (1994) 279–286.
[27] W. Wei, W. Chen, D.,G. Ivey, Rock salt-spinel structural transformation in anodically electrodeposited Mn-Co-O nanocrystals, Chem. Mater. 20 (2008) 1941–1947.
[28] B.J. Tan, K.J. Klabunde, P.M.A. Sherwood, XPS studies of solvated metal atom dispersed (SMAD) catalysts. Evidence for layered cobalt-manganese particles on alumina and silica, J. Am. Chem. Soc. 113 (1991) 855–861.
[29] K.M. Shaju, G.V.S. Rao, B.V.R. Chowdari, Performance of layered Li $(Ni_{1/3}Co_{1/3}Mn_{1/3})O_2$ as cathode for Li-ion batteries, Electrochim. Acta 48 (2002) 145–151.
[30] B.J. Hwang, Y.W. Tsai, D. Carlier, G. Cender, A combined computational/experimental study on $LiNi_{1/3}Co_{1/3}Mn_{1/3}O_2$, Chem. Mater. 15 (2003) 3676–3682.
[31] J.-M. Kim, H.-T. Chung, Role of transition metals in layered Li[Ni ,Co, Mn]O_2 under electrochemical operation, Electrochim. Acta 49 (2004) 3573–3580.
[32] P.F. Wang, H.R. Yao, X.Y. Liu, J.N. Zhang, L. Gu, X.Q. Yu, Y.X. Yin, Y.G. Guo, Ti-substituted $NaNi_{0.5}Mn_{0.5-x}Ti_xO_2$ cathodes with reversible O3-P3 phase transition for high-performance sodium-ion batteries, Adv. Mater. 29 (2017).
[33] D. Yuan, X. Liang, L. Wu, Y. Cao, X. Ai, J. Feng, H. Yang, A honeycomb-layered $Na_3Ni_2SbO_6$: a high-rate and cycle-stable cathode for sodium-ion batteries, Adv. Mater. 26 (2014) 6301–6306.
[34] Y. You, S.O. Kim, A. Manthiram, A honeycomb-layered oxide cathode for sodium-ion batteries with suppressed P3-O1 phase transition, Adv. Energy Mater. 7 (2017), 1601698.
[35] D.D. Yuan, Y.X. Wang, Y.L. Cao, X.P. Ai, H.X. Yang, Improved electrochemical performance of Fe-substituted $NaNi_{0.5}Mn_{0.5}O_2$ cathode materials for sodium-ion batteries, ACS Appl. Mater. Interfaces 7 (2015) 8585–8591.
[36] Y. Wen, B. Wang, G. Zeng, K. Nogita, D. Ye, L. Wang, Electrochemical and structural study of layered P2-type $Na_{2/3}Ni_{1/3}Mn_{2/3}O_2$ as cathode material for sodium-ion battery, Chem. Asian. J. 10 (2015) 661–666.
[37] J. Deng, W.-B. Luo, X. Lu, Q. Yao, Z. Wang, H.-K. Liu, H. Zhou, S.-X. Dou, High energy density sodium-ion battery with industrially feasible and air-stable O3-type layered oxide cathode, Adv. Energy Mater. 8 (2018), 1701610.
[38] H. Xu, J. Zong, S. Chen, F. Ding, Z.-W. Lu, X.-J. Liu, Synthesis and evaluation of $NaNi_{0.5}Co_{0.2}Mn_{0.3}O_2$ as a cathode material for Na-ion battery, Ceram. Int. 42 (2016) 12521–12524.
[39] L.G. Chagas, D. Buchholz, C. Vaalma, L. Wu, S. Passerini, P-type $Na_xNi_{0.22}Co_{0.11}Mn_{0.66}O_2$ materials: linking synthesis with structure and electrochemical performance, J. Mater. Chem. A 2 (2014) 20263–20270.
[40] S. Doubaji, M. Valvo, I. Saadoune, M. Dahbi, K. Edström, Synthesis and characterization of a new layered cathode material for sodium ion batteries, J. Power Sources 266 (2014) 275–281.
[41] X. Sun, X.-Y. Ji, H.-Y. Xu, C.-Y. Zhang, Y. Shao, Y. Zang, C.-H. Chen, Sodium insertion cathode material $Na_{0.67}[Ni_{0.4}Co_{0.2}Mn_{0.4}]O_2$ with excellent electrochemical properties, Electrochim. Acta 208 (2016) 142–147.
[42] D. Yuan, W. He, F. Pei, F. Wu, Y. Wu, J. Qian, Y. Cao, X. Ai, H. Yang, Synthesis and electrochemical behaviors of layered $Na_{0.67}[Mn_{0.65}Co_{0.2}Ni_{0.15}]O_2$ microflakes as a stable cathode material for sodium-ion batteries, J. Mater. Chem. A 1 (2013) 3895.
[43] K. Kaliyappan, J. Liu, A. Lushington, R. Li, X. Sun, Highly stable $Na_{2/3}(Mn_{0.54}Ni_{0.13}Co_{0.13})O_2$ cathode modified by atomic layer deposition for sodium-ion batteries, ChemSusChem 8 (2015) 2537–2543.
[44] V.S. Rangasamy, L. Zhang, J.W. Seo, J.-P. Locquet, S. Thayumanasundaram, Enhanced electrochemical performance of $Na_{2/3}[Mn_{0.55}Ni_{0.30}Co_{0.15}]O_2$ positive electrode in sodium-ion batteries by functionalized multi-walled carbon nanotubes, Electrochim. Acta 237 (2017) 29–36.